ACS APPLIED MATERIALS & INTERFACES

Research Article

www.acsami.org

In Situ Generation of Electron Donor to Assist Signal Amplification on Porphyrin-Sensitized Titanium Dioxide Nanostructures for Ultrasensitive Photoelectrochemical Immunoassay

Jian Shu, Zhenli Qiu, Junyang Zhuang, Mingdi Xu, and Dianping Tang*

Key Laboratory of Analysis and Detection for Food Safety (MOE & Fujian Province), Institute of Nanomedicine and Nanobiosensing, Department of Chemistry, Fuzhou University, Fuzhou 350108, People's Republic of China

ABSTRACT: An ultrasensitive photoelectrochemical (PEC) immunoassay protocol for quantitative detection of low-abundant proteins at a low potential was designed by utilizing porphyrin-sensitized titanium dioxide (TiO_2) nanostructures. Experimental results demonstrated that the water-soluble 5,10,15,20-tetra(4-sulfophenyl)-21*H*,23*H*-porphyrin (TSPP) could be bound onto titanium dioxide via the sulfonic group. TSPP-sensitized TiO_2 nanostructures exhibited better photoelectrochemical responses and stability in comparison with TiO_2 nanoparticles alone under continuous illumination. Using carcinoembryonic antigen (CEA) as a model analyte, a typical PEC immunosensor by using TSPP-TiO_2 as the affinity support of anti-CEA capture antibody (Ab_1) to facilitate the improvement of photocurrent response was developed. Bioconjugates of secondary antibody and glucose oxidase with gold nanoparticles (Ab_2/GOx-AuNPs) was introduced by an antigen−antibody immunoreaction. AuNP acted as a powerful scaffold to bind with bioactive molecules, while GOx catalyzed glucose to in situ generate hydrogen peroxide (H_2O_2). The generated H_2O_2 as a sacrificial electron donor could be oxidized by the photogenerated holes to assist the signal amplification at a low potential under light excitation, thus eliminating interference from other species coexisting in the samples. Under optimal conditions, the PEC immunosensor showed a good linear relationship ranging from 0.02 to 40 ng mL^{-1} with a low detection limit of 6 pg mL^{-1} CEA. The precision, reproducibility, and specificity were acceptable. In addition, the method accuracy was also evaluated for quantitatively monitoring human serum samples, giving results matching with the referenced CEA ELISA kit.

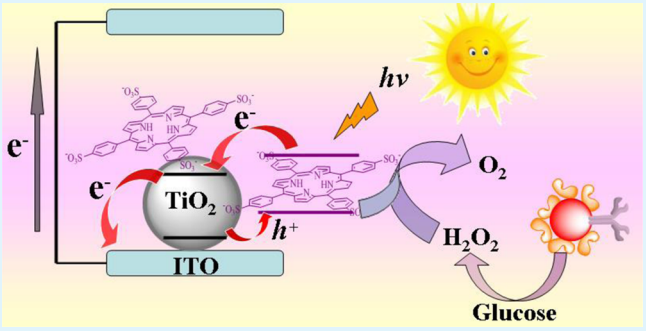

KEYWORDS: *photoelectrochemical immunoassay, porphyrins, carcinoembryonic antigen, titanium dioxide nanostructures, hybrid nanostructures, photocurrent*

1. INTRODUCTION

The increasing demands of food security, pharmaceutical, and biomedical analyses promote the development of sensitive and accurate detection methods.[1] As a newly emerging analytical method, photoelectrochemical (PEC) technique has received substantial attention and rapid development in the bioanalysis because of its unmatched merits.[2,3] First of all, PEC bioanalysis usually employs two separate forms of signal for excitation and detection, thus endowing it with a low background signal and ultrahigh sensitivity. Second, the applied potential is designable to some extent during the detection process due to the existence of electron−hole pairs, as well as the characteristic of strong oxidation reduction in semiconductors.[4] Because performance of PEC bioanalysis relies heavily on the photoactive materials, biomolecular conjugation with photoactive materials not only affects the photovoltaic efficiency and stability of photoactive materials, but also affects biomolecular activity. Thus, the signal amplified strategies and biosensing format are limited, which will struggle to satisfy the demand of practical detection. Despite the progress that has been made, the investigation on PEC immunoassay is still in infancy. On the other hand, owing to the demand for ultrasensitive detection of low-abundant proteins, it is essential to explore innovative photoactive material to significantly improve the photoelectric conversion efficiency and stability of PEC sensor. It is also necessary to develop new formats in PEC immunoassay and provide universal routes for success expanding the PEC applications.

To date, many semiconductor nanomaterials such as CdS, CdSe, ZnO, and TiO_2 have been used to construct PEC sensors.[5] Among these semiconductors, TiO_2 nanostructures have been extensively investigated as the significant photoelectrochemical materials due to the multitudinous superiority such as excellent photoelectric effect, light corrosion resistance, nontoxicity and cheap availability. However, TiO_2 must be excited by ultraviolet light ($\lambda \leq 387$ nm) because of the large band gap (3.2 eV for anatase), only about 4% of the incoming solar energy utilize by TiO_2 limited photoelectric effect, which

Received: September 16, 2015
Accepted: October 9, 2015
Published: October 9, 2015

DOI: 10.1021/acsami.5b08742
ACS Appl. Mater. Interfaces 2015, 7, 23812−23818

Scheme 1. Schematic Illustration of in Situ Generation of Electron Donor (H_2O_2) on Porphyrins-Sensitized Titanium Dioxide (TiO_2) Nanostructures for Low-Potential and Ultrasensitive Photoelectrochemical Immunoassay toward Target CEA

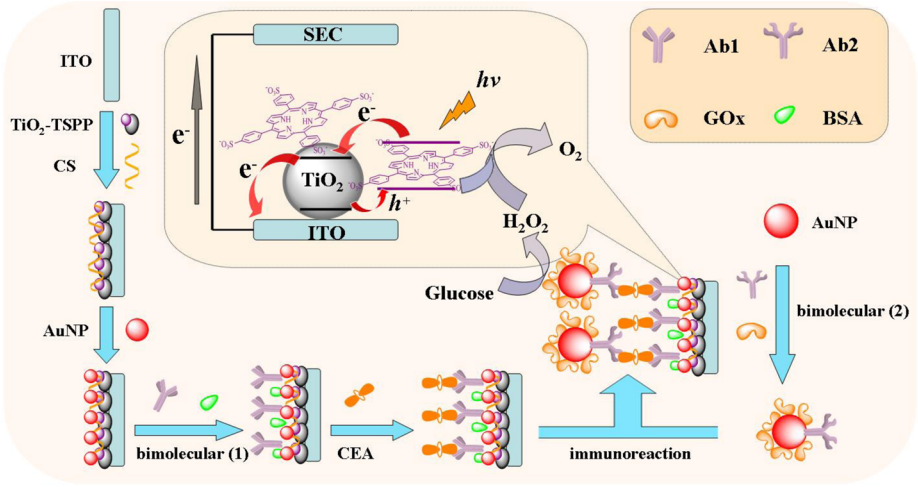

prevents it from being a potential visible light harvester. And UV irradiation also impedes its application in PEC bioanalysis because UV light could lower activity of biomolecules. On the other hand, recombination of electron and hole further reduce photoelectric effect. Thus, various chemical methods such as metal deposition,[6,7] semiconductor compound,[8,9] and dye sensitization[10] are employed to improve the performance. Porphyrins as the structural analogues of chlorophyll are considered as efficient sensitizers to harvest light on the surface of semiconductors. Porphyrins exist in the natural world as ferroheme of animals and chlorophyll of plants and have become a research hotspot in frontier fields such as dye-sensitized solar cells,[11,12] mimic enzyme,[13] and photodynamic therapy.[14,15] Due to the ultrafast electron injection and slow charge recombination kinetics, pulse large absorption in the visible region because the existence of the delocalized π electrons system. Water-soluble 5,10,15,20-tetra(4-sulfophenyl)- 21*H*,23*H*-porphyrin (TSPP) possesses good affinity to biological molecules due to the existence of the sulfonic group. More importantly, sulfonic groups can make porphyrin stable combination with nanoparticle that beneficial to the electron transfer.

In this work, large band gap semiconductor TiO_2 nanoparticles are combined with TSPP as an advanced photoactive material to enhanced photocurrent response and stability. Our motivations were not only to explore the performance of the advanced material on the photocurrents, but also study the possible application in immunoassay. Experimental results demonstrate that the complexes provided significant advantages for enhancing light absorption and charge separation which greatly improve the photocurrent intensity and stability. On the basis of specific recognition between antibody and antigen, we designed an ultrasensitive PEC immunoassay for the detection of biomarkers at a low potential. Using carcinoembryonic antigen (CEA) as a model analyte, a stable and ultrasensitive PEC immunosensor for the detection of CEA is fabricated by stepwise modification of TSPP-TiO_2, capture antibody, and glucose oxidase (GOx)/secondary antibody-conjugated gold nanoparticle. GOx serves as a catalyst to in situ generate H_2O_2 through the decomposition of glucose for the signal amplification. H_2O_2 acts as a sacrificial electron donor to scavenge the photogenerated holes to assist signal amplification at a lower potential. The improved photocurrent conversion efficiency and intensity of photocurrent can be further amplified by H_2O_2 and the developed immunosensor possess a high sensitivity and a wide potential optional range to avoid the interference from coexist species in real sample.

2. EXPERIMENTAL SECTION

Material and Reagent. CEA standards and monoclonal rabbit antihuman CEA capture antibody (denoted as Ab_1) were purchased from Biocell Biotechnol. Inc. (Zhengzhou, China). Polyclonal rabbit antihuman CEA detection/secondary antibody (denoted as Ab_2, Beijing Biosynth. Biotechnol., Inc., China), 5,10,15,20-Tetra (4-sulfophenyl)-21*H*,23*H*-porphyrin (denoted as TSPP, Taiwan Luminescence Technol. Inc., China), bovine serum albumin (BSA, Shanghai Sinopharm Chem. Inc., China) and glucose oxidase (GOx, Type X-S, lyophilized powder, 100−250 units mg^{-1} solid, Sigma-Aldrich) were used throughout this work. Titanium dioxide (TiO_2) nanoparticles and chitosan were acquired from Alfa Aesar (Shanghai, China). Gold nanoparticles (AuNPs, 16 nm in diameter) were prepared and characterized in our previous work.[16] Ultrapure water from a Milli-Q purification system was used in all runs (≥18.2 MΩ cm^{-1}, Millipore). Other chemicals were of analytical grade. Phosphate-buffered saline (PBS) solution was prepared by adding 0.1 M NaCl into mixture of 0.1 M Na_2HPO_4 and 0.1 M KH_2PO_4.

Preparation of TSPP-Sensitized TiO_2 Nanoparticles (TSPP-TiO_2). TiO_2 aqueous suspension (0.75 mg mL^{-1}, 2.0 mL) was initially dropped into 4 mL dimethylformamide (DMF) containing 0.3 mg TSPP, and the mixture was then sonicated for 20 min at room temperature. Following that, the suspension was heated at 80 °C for 5 h. Finally, the obtained suspension was centrifuged (15 min at 10 000*g*) and washed with distilled water to remove the unabsorbed TSPP. The as-prepared TSPP-sensitized TiO_2 nanoparticles (denoted as TSPP-TiO_2) were dispersed into DMF (~2.0 mg mL^{-1}) for the subsequent use.

Preparation of GOx/Ab_2-Conjugated AuNP (GOx-AuNP-Ab_2). Glucose oxidase and anti-CEA detection antibody-conjugated gold nanoparticle (denoted as GOx-AuNP-Ab_2) was prepared similar to our previous work.[16] Initially, the as-prepared gold colloids were adjusted to pH 8.0−8.5 by using Na_2CO_3 aqueous solution. Thereafter, 10 μL of Ab_2 (0.1 mg mL^{-1}) and 10 μL of GOx (1.0 mg mL^{-1}) were simultaneously added to the resulting gold colloids (1.0 mL, 24 nM). Following that, the suspension was gently shaken for 6 h on a shaker at 4 °C. During this process, Ab_2 detection antibody and GOx were covalently conjugated to gold nanoparticles on the basis of the interaction between cysteine/NH_3^+-lysine residues of the proteins and nanogold particles. The unconjugated biomolecules including Ab_2 and

DOI: 10.1021/acsami.5b08742
ACS Appl. Mater. Interfaces 2015, 7, 23812−23818

GOx were removed by centrifugation and washing with pH 7.4 PBS. Finally, the as-prepared GOx-AuNP-Ab_2 was redispersed into pH 7.4 PBS (800 μL, 0.1 M) containing BSA (1.0 wt %) and sodium azide (0.1 wt %).

Fabrication of Photoelectrochemical Immunosensor. In this work, indium tin oxide (ITO, 5.0 wt % In_2O_3 + SnO_2) was used for the construction of the photoelectrochemical immunosensor. Initially, 6.0 μL of TSPP-TiO_2 suspension in the DMF (2.0 mg mL^{-1}) was dropped to a cleaned ITO electrode (0.16 cm^2). After being dried at room temperature, the same-amount TSPP-TiO_2 colloids were coated on the same region again (i.e., two times for the coating process). Following that, 6.0 μL of 5.0 wt % chitosan in the acetic acid was thrown on the TSPP-TiO_2-modified ITO and dried at room temperature to avoid the exfoliation of TSPP-TiO_2. After being washed with distilled water, 6.0 μL of gold colloids (0.24 μM) was dropped on the resulting ITO. During this process, colloidal gold was immobilized onto the chitosan-modified ITO through the interaction between $-NH_3^+$ and gold nanoparticles. Subsequently, 6.0 μL of 1.0 mg mL^{-1} Ab_1 capture antibody was introduced and incubated for 6 h at 4 °C. Finally, the as-prepared immunosensor (i.e., Ab_1/AuNP/TSPP-TiO_2/ITO) was stored at 4 °C when not in use after being blocked with 2.5 wt % BSA for 1 h at 37 °C.

Photoelectrochemical Measurement for Target CEA. Scheme 1 provides an illustration of in situ generation of electron donor on porphyrins-sensitized TiO_2 nanostructures for low-potential and ultrasensitive photoelectrochemical immunoassay toward target CEA. All photoelectrochemical measurements were performed by using an AutoLab electrochemical workstation (μAUTIII.FRA2.v, The Netherlands). The detection system consisted of a modified ITO working electrode, a platinum wire counter electrode and an Ag/AgCl reference electrode. The immunoreaction and photocurrent measurement were described in detail as follows: (1) 10 μL of CEA sample/standard with different concentrations was thrown on the immunosensor and incubated 30 min at room temperature; (2) 10 μL of the above-prepared GOx-AuNP-Ab_2 was casted and incubated under the same conditions to form the sandwiched immunocomplex; and (3) the photocurrent was measured in pH 6.5 PBS containing 1.0 mM glucose with light excitation at the applied potential of 0 V. After each step, the immunosensor was washed with pH 7.4 PBS.

3. RESULTS AND DISCUSSION

Characterization of TSPP-TiO_2. Transmission electron microscopy (TEM) was first utilized to characterize the topological profiles of TiO_2 nanoparticles and TSPP-TiO_2 hybrid nanostructures. Figure 1 shows the typical TEM images of TiO_2 nanoparticles before and after modification with TSPP, respectively. As shown in Figure 1A, pure TiO_2 nanoparticles were easily aggregated together to form larger nanostructures. Meanwhile, we observed that the agglomerated nanoscales displayed discernible surface with an average size of 25 nm for single TiO_2 nanoparticle (Figure 1B). When TiO_2 nanoparticles were functionalized with TSPP, favorably, the dispersity was largely improved relative to TiO_2 nanoparticles (Figure 1C). Moreover, the surface became rougher with the blurred contour (Figure 1D), which was characteristic of the organic attachment. In comparison with TiO_2 nanoparticles alone (Figure 1B), the size of the aggregated nanostructures after modification was obviously smaller (Figure 1D), which was beneficial for the formation of homogeneous film on the electrode. The morphological change preliminarily suggested that TSPP molecules were bond onto the surface of TiO_2 nanoparticles.

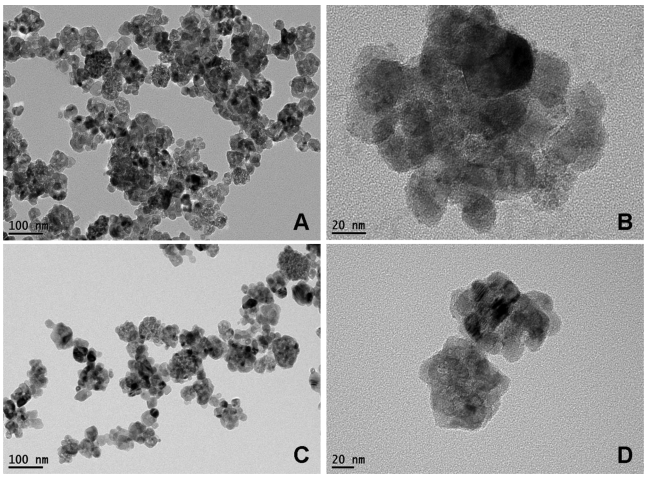

Figure 1. TEM images of (A and B) TiO_2 nanoparticles and (C and D) TSPP-TiO_2 nanostructures. Images B and D are magnified TEM images of TiO_2 nanoparticles and TSPP-TiO_2, respectively.

To further demonstrate the formation of TSPP-TiO_2 hybrid nanostructures, we also used Fourier transform infrared spectroscopy (FTIR) to confirm the bonding situation of TSPP-TiO_2 (Figure 2A). Typically, the bonding situation directly influences the electron transfer between photosensitizer and TiO_2 nanoparticles, which indirectly affects the photoelectric efficiency.[17] As seen from curve c in Figure 2A, most typical characteristic peaks for TSPP (curve a) and TiO_2 nanoparticles (curve b) simultaneously appeared after formation of TSPP-TiO_2 hybrid nanostructures. The shapes of the infrared absorption bands at 1040, 805, and 735 cm^{-1} derived from the C−H bending vibration of TSPP, while the characteristic absorption bands at 1630 and 1480 cm^{-1} originated from the skeletal vibration of the porphyrins. Significantly, the characteristic peaks for sulfonic groups at 1165, 1120, and 1037 cm^{-1} disappeared or shifted at TSPP-TiO_2 relative to TSPP and TiO_2 nanoparticles alone. These results also revealed that the as-synthesized TSPP-TiO_2 hybrid nanostructures were formed by the covalent binding of TiO_2 nanoparticles with anchoring groups (SO^{3-}) of TSPP rather than only physical adsorption, which was in accordance with previous report.[5]

In addition, UV−vis absorption spectroscopy was also employed for demonstration of TSPP-TiO_2 formation (Figure 2B). As shown in curve a, TSPP with a narrow band gap of 2.8 eV exhibited an intense Soret band at 413 nm (3.27×10^5 M^{-1} cm^{-1}), and four Q bands at 515 nm (1.3×10^4 M^{-1} cm^{-1}), 552 nm (5.9×10^3 M^{-1} cm^{-1}), 580 nm (5.5×10^3 M^{-1} cm^{-1}) and 632 nm (3.2×10^3 M^{-1} cm^{-1}) in pH 7.0 aqueous solutions.[18] The large molar absorption coefficient and wide spectral response range provided the potential promising in photovoltaic materials. In contrast, almost no absorption peaks were observed within 400−700 nm at TiO_2 nanoparticles, while the absorbance increased with the decreasing wavelength in the UV region (curve b). When TSPP molecules were conjugated to TiO_2 nanoparticles, the hybrid nanostructures exhibited a wide peak with a 19 nm bathochromic shift at original Soret band (curve c). Compare with TiO_2 nanoparticles (curve b), the absorbance of the as-synthesized TSPP-TiO_2 apparently increased within the whole visible range. The shift in the characteristic peak and the increment in the absorbance further confirmed that the interaction between TSPP and TiO_2 nanoparticles mainly came from the chemical linkage.

Before monitoring the photoelectric characteristics and possible application of the as-synthesized TSPP-TiO_2 nanostructures in the immunoassays, several puzzling concerns

DOI: 10.1021/acsami.5b08742
ACS Appl. Mater. Interfaces 2015, 7, 23812−23818

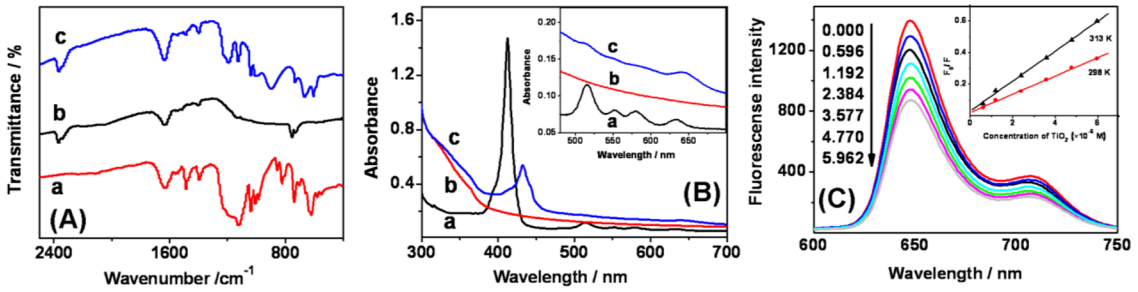

Figure 2. (A) FTIR spectra of (a) TSPP, (b) TiO_2, and (c) TSPP-TiO_2; (B) UV−vis absorption spectra of (a) TSPP, (b) TiO_2, and (c) TSPP-TiO_2, and (inset) magnification of UV−vis absorption spectra in the visible range; (C) fluorescence spectra of TSPP (6.5×10^{-5} M) in the presence of various concentrations of TiO_2 ($\times 10^{-4}$ M) under 313 K with excitation wavelength at 414 nm and (inset) Stern−Volmer plots of fluorescence quenching under different temperatures.

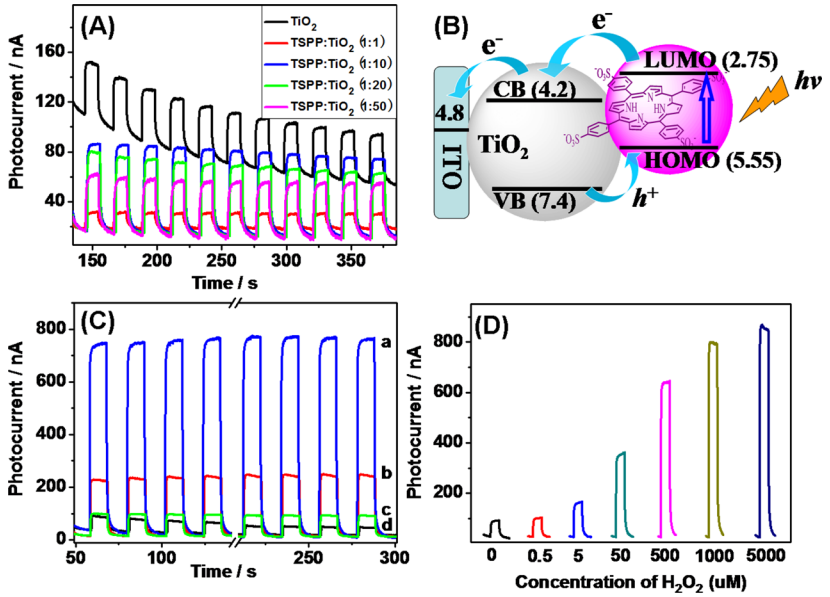

Figure 3. (A) Photocurrent responses of various amount TSPP-sensitized TiO_2; (B) energy level diagram and electron-transfer mechanisms of the nanostructures (all values given in eV); (C) photocurrent responses of TSPP-TiO_2 (a and c) and TiO_2 (b and d) in the absence (c and d) and the presence (a and b) of H_2O_2; and (D) photocurrents of TSPP-TiO_2-modified ITO toward different-concentration H_2O_2.

should be clarified as follows: (1) whether TSPP, as a kind of photosensitizer, could strengthen the efficiency of luminous energy because good absorption in the visible region and the close integration with the hybrid nanostructures were essential, (2) whether the excited state of TSPP could fast transfer the electrons into the conduction band of the hybrid nanostructures, and (3) whether the photoelectrochemical response of the as-synthesized TSPP-TiO_2 was superior to that of TiO_2 nanoparticles alone. Although the electron transition occurring at porphyrin ring can be partially illustrated on the basis of strong absorbance in the visible region, the amplified efficiency is not adequately supported. In this regard, fluorescence spectrum was employed (Figure 2C). A strong fluorescent peak at 655 nm and a weak fluorescent peak at 718 nm were achieved at pure TSPP, which was excited by 414 nm. The fluorescence intensity of TSPP linearly decreased with the increasing TiO_2 nanoparticles. The reason might be attributed to quenching of TiO_2 nanoparticles, suggesting an efficient nonradiative energy transfer from the excited state TSPP to TiO_2 nanoparticles.[17] Moreover, with the increasing temperature, TiO_2 revealed enhanced quenching efficiency, which was characteristic of dynamic quenching. According to the previous literatures,[17,19] the quenching rate constant for the quenching process was found to be 1.78×10^{11} M^{-1} s^{-1}, such value represented the electron transfer from lowest unoccupied molecular orbital (LUMO) of TSPP to the conduction band of TiO_2 and the electron transfer was an ultrafast process. In addition, it could also eliminate self-quenching that caused by accumulation of TSPP on the semiconductor surface. Use of porphyrin sensitized wide band gap semiconductor nanoparticle might provide a feasible mean to modulate charge recombination in the photochemical sensors.

Photocurrent Response of TSPP-TiO_2. Typically, the intensity of photocurrent greatly depends on the porphyrin amount because of only very close to the surface of TiO_2 nanoparticles. Logically, another important question arises to whether the sensitizer could inject the electron into the conduction band of TiO_2 nanoparticles. Thus, the effect of various-mass ratios of TSPP and TiO_2 ranging from 1.0 to 50 wt % at interval of 10% on the performance of photocurrent response was investigated (Figure 3A). Results clearly suggested that both the TiO_2 and different-proportion TSPP sensitizing TiO_2 modified ITO electrode showed responsive current under visible light excitation. It was easy to observe irrespective percentage of TSPP, a high stability and little change of photocurrent under light repeatedly irradiates for a

DOI: 10.1021/acsami.5b08742
ACS Appl. Mater. Interfaces 2015, 7, 23812−23818

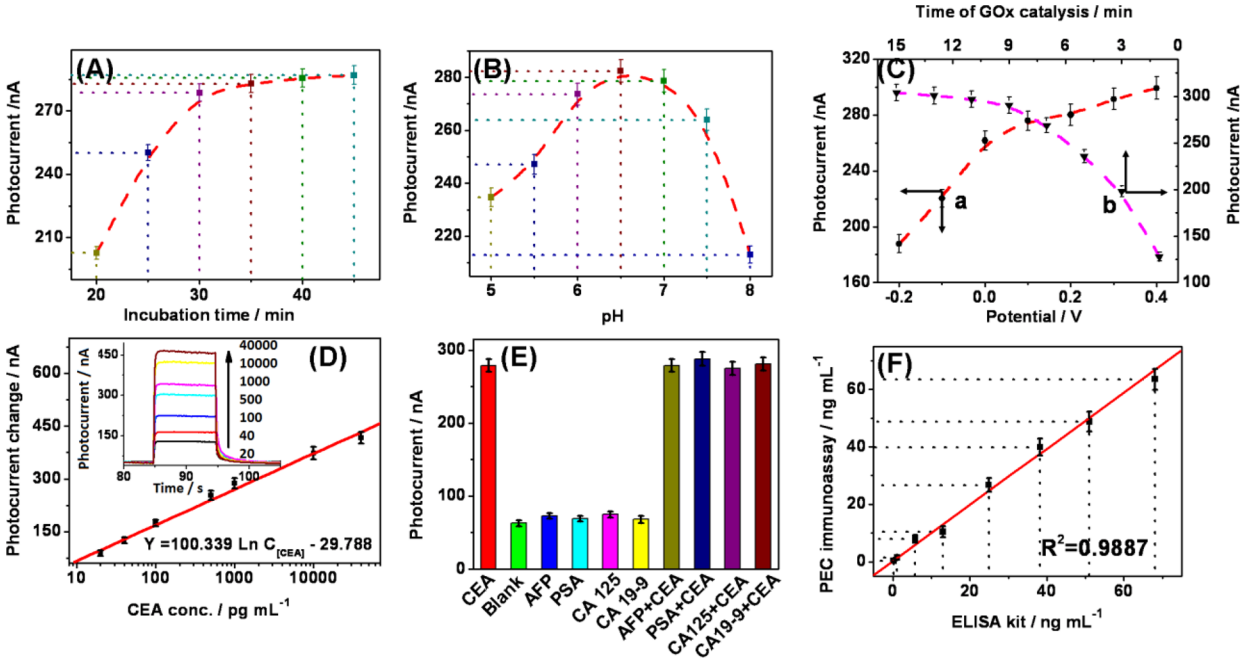

Figure 4. Influence of (A) incubation time for the antigen−antibody reaction, (B) pH of detection solution, and (C, a) applied potential and (b) GOx catalytic time on the current of the photoelectrochemical immunosensor (1.0 ng mL^{-1} CEA used in all cases). (D) Calibration curve of the photoelectrochemical immunosensor toward CEA standards with different concentrations and (inset) corresponding photocurrent responses. (E) Specificity of the photoelectrochemical immunosensor against 1.0 ng mL^{-1} CEA, 10 ng mL^{-1} AFP, 10 ng mL^{-1} PSA, 10 ng mL^{-1} CA, and 125 and 10 ng mL^{-1} CA 19−9; the mixture contained only these interfering materials. (F) Comparison of the results for human CEA serum samples obtained between the photoelectrochemical immunoassay and the referenced CEA ELISA kit.

long time. In contrast, the photocurrent of TiO_2 gradually reached steady until 200 s, and photocurrent decreased in the same condition. However, only a proper proportion (1:10) of TSPP could obtain the maximum photocurrent intensity and simultaneously keep the excellent stability, which was attributed to the fact that less sensitizer could harvest more light and inhibit the recombination of electron−hole pairs, while multilayer adsorption of sensitizer could hinder light absorbance and block the electron transport. Under the optimal proportion, the photocurrent intensity of TSPP-TiO_2 (86.2 nA) increased 20% in comparison with that of pure TiO_2 (71.6 nA). Because TiO_2 sensitized by TSPP could obviously shorten the time to reach the steady state and promote photocurrent stability, it was conducive to construct a biosensor for accurate and rapid detection.

To understand the electron transfer and sensitization mechanism, we gathered further information about the energy level of TSPP and TiO_2.[20−22] Due to the narrower band gap (2.8 eV), electrons of TSPP could be excited from the ground state to the excited state under the irradiation of visible light. The excited state energy of TSPP was higher than conduction band energy level of TiO_2. The effective matching of energy levels between TSPP and TiO_2 suggested fast electron transfer from the TSPP to the conduction band of TiO_2 was energetically favorable and could improve the photocurrent. On the basis of these results, a possible mechanism of signal generated from TSPP-TiO_2 under visible-light irradiation is shown in Figure 3B.

Furthermore, the improved photocurrent conversion efficiency and intensity of photocurrent could be further amplified by electron donor. H_2O_2 as a reducing agent could consume the hole of TiO_2 with low potential to suppression electron hole recombination under irradiation. Here, H_2O_2 was used to further amplify photocurrent (Figure 3C). In the presence of H_2O_2, the photocurrent of TSPP-TiO_2 increased 8-fold (750 nA, curve a) over that in the absence of H_2O_2 (96 nA, curve c), while the pure TiO_2 only increased 3-fold (232 nA, curve b) over that in the absence of H_2O_2 (78 nA, curve d) under the same conditions. Of course, the sensitivity of immunosensor, like most, depended on the change in the response values. Under the double action, the photocurrents of TSPP-TiO_2 and TiO_2 were magnified 9 and 3 times, respectively. It was reasonable to conclude that TiO_2 sensitized by TSPP could improve the sensitivity near 3 times in comparison with pure TiO_2. More importantly, compared with curves c and d, the stable advantage of TSPP-TiO_2 was apparent under light repeatedly irradiates for a long time. The photocurrent intensity of TSPP-TiO_2 was observed to increase with the increasing H_2O_2 concentration (Figure 3D). The response to H_2O_2 was sensitive enough that even 0.5 μM of H_2O_2 solution could result in an increase in photocurrent, even under 0 V potential. It was a key precondition for the development of ultrasensitive PEC immunoassay method. These results indicated that TSPP-TiO_2 could not only provide fast and stable response, but also dramatically improved sensitivity and could be turned on and off by controlling the light. The TSPP-TiO_2 shows promising as a photoactive material to construct PEC biosensor.

Optimization of Detection Conditions. To monitor the practical application of TSPP-TiO_2, we constructed a new photoelectrochemical immunosensor for the detection of CEA. H_2O_2, as electron donor to amplify the detectable signal, was generated by the labeled GOx on the detection antibody. Some factors influencing the photocurrent response of PEC immunosensor (e.g., incubation time, pH of detection solution, applied potential, and enzymatic catalytic time) were optimized. As shown in Figure 4A, the photocurrent increased with the

DOI: 10.1021/acsami.5b08742
ACS Appl. Mater. Interfaces 2015, 7, 23812−23818

extending incubation time and reached to a steady value at 30 min. Meanwhile, pH of detection solution also affected the activity of biomolecules. The photocurrent of PEC immunosensor showed a maximum photocurrent response at pH 6.5 (Figure 4B). Thus, pH 6.5 PBS and 30 min were used as the supporting electrolyte and incubation time for the antigen−antibody reaction, respectively.

Specially, the reaction time of GOx-catalyzed glucose was investigated from 0 to 15 min (Figure 4C, curve b), while the detection potential was monitored from −0.2 to +0.4 V (Figure 4C, curve a). The photocurrent sharply increased with the extending time because the time of GOx-catalyzed glucose directly influenced the amount of the generated H_2O_2. Because the photocurrent reached a steady value at 9 min, a long catalytic time did not significantly increase the response. With the continuous enhancement of detection potential, the change in the photocurrent was also obviously increased and gradually leveled off. The reason was attributed to the fact that the external voltage effectively prompted the separation of the photoelectrons from the vacancies. Favorably, glucose as the substrate does not interfere at the potential range. To expand the application for subsequent real sample, the potential at 0 V showed enough sensitivity for PEC detection of CEA (photocurrent at 0 V was 87.4% of that at +0.4 V). Thus, 0 V was chosen as the detection potential.

Analytical Performance. As described above, the shift in the photocurrent (ΔI) at the excitation light between on and off directly relies on H_2O_2 concentration. Thus, target CEA could be indirectly detected with a sandwiched immunoassay mode via GOx-mediated generation of H_2O_2 electron donor accompanying the photocurrent. As seen from the inset in Figure 4D, the photocurrent increased with the increasing target CEA in the sample under the optimal conditions. Meanwhile, we observed that the photocurrents linearly increased against the logarithm of CEA concentrations within the dynamic range of 0.02−40 ng mL^{-1} (Figure 4D). The detection limit (LOD) could be estimated to 6.0 pg mL^{-1} (S/N = 3). The linear regression equation could be fitted as follows: ΔI (nA) = 100.339 × $LnC_{[CEA]}$ − 29.788 (pg mL^{-1}, R^2 = 0.9959, n = 21). Such a high slope (i.e., sensitivity) in the regression equation originated from strong signal-amplified efficiency of PEC immunosensor on the basis of in situ generation of H_2O_2 electron donor by coupling with TSPP-TiO_2.

Further, we studied the reproducibility and precision of PEC immunosensor through repeatedly detecting 3 CEA standards including 0.05, 1.0, and 20 ng mL^{-1}. As analyzed from our experimental results, the relative standard deviations (RSDs) by using the same-batch GOx-AuNP-Ab_2 and PEC immunosensors were 8.3, 6.5, and 7.6% (n = 3) toward the above-mentioned three samples, respectively. By using different-batch GOx−AuNP−Ab_2 and immunosensors, the RSDs were 8.9, 10.6 and 9.3% (n = 3) toward 0.05, 1.0, and 20 ng mL^{-1}, respectively. Hence, the reproducibility and precision of PEC immunosensor was satisfactory.

Next, the specificity of PEC immunosensor was also investigated by assaying other biomarkers, for example, cancer antigen 19−9 (CA 19−9), alpha-fetoprotein (AFP), cancer antigen 125 (CA 125), and prostate specific antigen (PSA). As shown in Figure 4E, the photocurrents of PEC immunosensor toward nontarget analytes were almost the same as the background signal. High photocurrents could only be achieved in the presence of target CEA. Significantly, the presence of nontarget analytes did not obviously affect the photocurrent responses of PEC immunosensor. In addition, the photocurrent could preserve 90.3% of the initial signal after being stored for 24 days. These results also revealed that our designed PEC immunosensors had high selectivity and long-term stability.

Monitoring of CEA in Human Serum Samples. To investigate the accuracy of our designed strategy, several human serum specimens containing target CEA were gifted from Department of Medical Diagnostics of Fujian Provincial Hospital (Fujian, China).The high-concentration CEA samples were diluted with pH 7.4 PBS to below 40 ng mL^{-1}. During the measurement, these samples were directly incubated with the as-prepared immunosensor. After that, they were monitored by the photoelectrochemical immunosensors, respectively. The CEA levels in these samples were calculated according to the above-mentioned linear regression equation in Figure 4D. Finally, the obtained results were compared with those from the referenced CEA ELISA kit (Sigma-Aldrich). As shown in Figure 4F, the regression equation could be fitted to y = 0.9531x + 0.027 (R^2 = 0.9887, n = 24), indicating a highly positive correlation between two methods. Therefore, the method accuracy should be acceptable, which could be preliminarily used for quantitative monitoring of target CEA concentration in the biological fluids.

4. CONCLUSIONS

This work provides a new photoactive nanomaterial with high photoelectric efficiency for advanced development of photoelectrochemical immunoassay. Compared with traditional PEC immunoassays, highlights of this study can be summarized as follows: (1) introduction of TSPP on titanium dioxide could strengthen the visible absorption and hinder the recombination of electron and hole, thereby improving the photocurrent conversion efficiency; (2) the photocurrent could be amplified through enzymatic catalysis accompanying in situ generated H_2O_2; and (3) the as-produced H_2O_2 as an electron donor could be oxidized at a low potential to assist the signal amplification since the photogenerated holes existed under light excitation. These characteristics carried forward the PEC immunosensor with high sensitivity and wide-potential range to avoid the potential interference, thereby representing an optional and versatile assay protocol for PEC immunoassay development.

AUTHOR INFORMATION

Corresponding Author

*Phone: +86-591-2286 6125. Fax: +86-591-2286 6135. E-mail: dianping.tang@fzu.edu.cn.

Notes

The authors declare no competing financial interest.

ACKNOWLEDGMENTS

This work was financially supported by the National Natural Science Foundation of China (41176079 and 21475025), the National Science Foundation of Fujian Province (2014J07001), Key Science Project (Type A) of the Fujian Provincial Department of Education of China (JA12021) and the Program for Changjiang Scholars and Innovative Research Team in University (IRT1116).

DOI: 10.1021/acsami.5b08742
ACS Appl. Mater. Interfaces 2015, 7, 23812−23818

REFERENCES

(1) Li, Y.; Ma, M.; Zhu, J. Dual-Signal Amplification Strategy for Ultrasensitive Photoelectrochemical Immunosensing of α-Fetoprotein. *Anal. Chem.* **2012**, *84*, 10492−10499.

(2) Zhao, W.; Xu, J.; Chen, H. Photoelectrochemical DNA Biosensors. *Chem. Rev.* **2014**, *114*, 7421−7441.

(3) Devadoss, A.; Sudhagar, P.; Terashima, C.; Nakata, K.; Fujishima, A. Photoelectrochemical Biosensors: New Insights into Promising Photoelectrodes and Signal Amplification Strategies. *J. Photochem. Photobiol., C* **2015**, *24*, 43−63.

(4) Sun, G.; Zhang, Y.; Kong, Q.; Ma, C.; Yu, J.; Ge, S.; Yan, M.; Song, X. Chemiluminescence Excited Paper-Based Photoelectrochemical Competitive Immunosensing Based on Porous ZnO Spheres and CdS Nanorods. *J. Mater. Chem. B* **2014**, *2*, 7679−7684.

(5) Tu, W.; Dong, Y.; Lei, J.; Ju, H. Low-potential Photoelectrochemical Bisoensing Using Porphyrin-Functionalized TiO_2 Nanoparticles. *Anal. Chem.* **2010**, *82*, 8711−8716.

(6) An, Y.; Tang, L.; Jiang, X.; Chen, H.; Yang, M.; Jin, L.; Zhang, S.; Wang, C.; Zhang, W. A Photoelectrochemical Immunosensor Based on Au-Doped TiO_2 Nanotube Arrays for the Detection of α-Synuclein. *Chem. - Eur. J.* **2010**, *16*, 14439−14446.

(7) Fan, W.; Jewell, S.; She, Y.; Leung, M. In Situ Deposition of Ag-Ag_2S Hybrid Nanoparticles onto TiO_2 Nanotube Arrays towards Fabrication of Photoelectrodes with High Visible Light Photoelectrochemical Properties. *Phys. Chem. Chem. Phys.* **2014**, *16*, 676−680.

(8) Lu, N.; Su, Y.; Li, J.; Yu, H.; Quan, X. Fabrication of Quantum-Sized CdS-Coated TiO_2 Nanotube Array with Efficient Photoelectrochemical Performance Using Modified Successive Ionic Layer Absorption and Reaction (SILAR) Method. *Sci. Bull.* **2015**, *6*, 1281−1286.

(9) Pang, X.; Pan, J.; Gao, P.; Wang, Y.; Wang, L.; Du, B.; Wei, Q. A Visible Light Induced Photoelectrochemical Aptsensor Constructed by Aligned ZnO@CdTe Core Shell Nanocable Arrays/Carboxylated g-C_3N_4 for the Detection of Proprotein Convertase Subtilisin/Kexin Type 6 Gene. *Biosens. Bioelectron.* **2015**, *74*, 49−58.

(10) Swierk, J.; Mallouk, T. Design and Development of Photoanodes for Water-Splitting Dye-Sensitized Photoelectrochemical Cells. *Chem. Soc. Rev.* **2013**, *42*, 2357−2387.

(11) Yella, A.; Lee, H.; Tsao, H.; Yi, C.; Chandiran, A.; Nazeeruddin, M.; Diau, E.; Yeh, C.; Zakeeruddin, S.; Grätzel, M. Porphyrin-Sensitized Solar Cells with Cobalt (II/III)-Based Redox Electrolyte Exceed 12% Efficiency. *Science* **2011**, *334*, 629−634.

(12) Mathew, S.; Yella, A.; Gao, P.; Humphry-Baker, R.; Curchod, B.; Ashari-Astani, N.; Tavernelli, I.; Rothlisberger, U.; Nazeeruddin, M.; Gratzel, M. Dye-Sensitized Solar Cells with 13% Efficiency Achieved through the Molecular Engineering of Porphyrin Sensitizers. *Nat. Chem.* **2014**, *6*, 242−247.

(13) Rebelo, S.; Linhares, M.; Simoes, M.; Silva, A.; Neves, M.; Cavaleiro, J.; Freire, C. Indigo Dye Production by Enzymatic Mimicking Based on an Iron (III) Porphyrin. *J. Catal.* **2014**, *315*, 33−40.

(14) Ethirajan, M.; Chen, Y.; Joshi, P.; Pandey, R. The Role of Porphyrin Chemistry in Tumor Imaging and Photodynamic Therapy. *Chem. Soc. Rev.* **2011**, *40*, 340−362.

(15) Schmitt, J.; Heitz, V.; Sour, A.; Bolze, F.; Ftouni, H.; Nicoud, J.; Flamigni, L.; Ventura, B. Diketopyrrolopyrrole-Porphyrin Conjugates with High Two-Photon Absorption and Singlet Oxygen Generation for Two-Photon Photodynamic Therapy. *Angew. Chem., Int. Ed.* **2015**, *54*, 169−173.

(16) Zhang, B.; Liu, B.; Tang, D.; Niessner, R.; Chen, G.; Knopp, D. DNA-Based Hybridization Chain Reaction for Amplified Bioelectronic Signal and Ultrasensitive Detection of Proteins. *Anal. Chem.* **2012**, *84*, 5392−5399.

(17) Sarkar, S.; Makhal, A.; Bora, T.; Lakhsman, K.; Singha, A.; Dutta, J.; Pal, S. Hematoporphyrin-ZnO Nanohybrids: Twin Applications in Efficient Visible-Light Photocatalysis and Dye-Sensitized Solar Cells. *ACS Appl. Mater. Interfaces* **2012**, *4*, 7027−7035.

(18) Aggarwal, L.; Borissevitch, I. On the Dynamics of the $TSPP_4$ Aggregation in Aqueous Solutions: Successive Formation of H and J Aggregates. *Spectrochim. Acta, Part A* **2006**, *63*, 227−233.

(19) Kathiravan, A.; Anbazhagan, V.; Asha Jhonsi, M.; Renganathan, R. Fluorescence Quenching of Meso-tetrakis (4-Sulfonatophenyl) Porphyrin by Colloidal TiO_2. *Spectrochim. Acta, Part A* **2008**, *70*, 615−618.

(20) Zhu, R.; Jiang, C.; Liu, B.; Ramakrishna, S. Highly Efficient Nanoporous TiO_2-Polythiophene Hybrid Solar Cells Based on Interfacial Modification Using a Metal-Free Organic Dye. *Adv. Mater.* **2009**, *21*, 994−1000.

(21) Miyairi, K.; Itoh, E.; Hashimoto, Y. Photovoltaic Properties of Double Layer Devices Consisting of Titanium Dioxide and Porphyrin Dispersed Hole Transporting Material Layer. *Thin Solid Films* **2003**, *438*, 147−152.

(22) Perez-Morales, M.; de Miguel, G.; Bolink, H.; Martin-Romero, M.; Camacho, L. Soret Emission from Water-Soluble Porphyrin Thin Films: Effect on the Electroluminescence Response. *J. Mater. Chem.* **2009**, *19*, 4255−4260.

DOI: 10.1021/acsami.5b08742
ACS Appl. Mater. Interfaces 2015, 7, 23812−23818